energies

MDPI

Article

Comparative Analysis of Flow Behavior and Geochemical Impact of CO_2 and Hydrogen in Lithuanian Saline Aquifer: A Simulation and Experimental Study

Shruti Malik [1], Parsa Alimohammadiardakani [2] and Mayur Pal [1,*]

[1] Department of Mathematical Modeling, Kaunas University of Technology, 44249 Kaunas, Lithuania; shruti.malik@ktu.lt
[2] Department of Production Engineering, Kaunas University of Technology, 44249 Kaunas, Lithuania; parsa.alimohammadiardakani@ktu.edu
* Correspondence: mayur.pal@ktu.lt

Abstract

Lithuania covers the deepest parts of the Baltic basin and contains many reservoirs that have been explored for Hydrocarbon production and gas storage projects, including CO_2 and hydrocarbon gas storage. Studies have also been conducted to assess the storage potential of these reservoirs for gases like CO_2 and Hydrogen. In the studies, four saline aquifers, including Syderiai, Vaskai, and D11, and depleted hydrocarbon reservoirs in the Gargzdai structure were evaluated for potential CO_2 storage. However, the long-term fate of these gases' migration at the field scale has not been reported previously. In response to the existing gap, this study aims to evaluate the risks and challenges associated with subsurface CO_2 and Hydrogen storage by conducting numerical simulations at two injection rates, of fluid migration, pH variations, and geomechanical responses using the tNavigator platform, complemented by laboratory experiments on outcrops representative of Syderiai formation, to achieve a detailed understanding of geochemical interactions between rocks and fluids. The results reveal distinct gas-specific behaviors: CO_2 exhibits enhanced solubility trapping, density-driven convective mixing, and pronounced pH reduction, whereas Hydrogen demonstrates rapid buoyant migration, higher pressure buildup, and negligible geochemical reactivity. Both gases demonstrate short-term storage viability in the Syderiai aquifer under the modeled conditions, with pressure and total vertical stress remaining below the bottom-hole pressure limit of 450 bars. This integrated simulation and experimental study enhances our understanding of Lithuanian reservoirs for the safe, long-term storage of both CO_2 and Hydrogen.

Keywords: CO_2 storage; Hydrogen storage; Lithuanian saline aquifer; mechanistic modeling; flow behavior; geomechanical study; geochemical changes

Academic Editor: Dameng Liu

Received: 30 November 2025
Revised: 2 January 2026
Accepted: 8 January 2026
Published: 11 January 2026

1. Introduction

The urgency to mitigate climate change has intensified global efforts toward renewable energy technologies like green Hydrogen and Carbon Capture, Utilization, and Storage (CCUS) [1]. Within the Baltic Sea Region (BSR), several countries—including Latvia, Estonia, Finland, Sweden, and Norway—have advanced research and demonstration activities in CCUS and Hydrogen [2–5]. However, Lithuania has remained largely underrepresented in this field despite its geological potential. The deepest part of the Baltic basin lies in

Lithuania [2,5] and has significant storage potential, as assessed in previous studies estimating CO_2 storage capacity in Lithuanian reservoirs [5–7]. The Baltic Basin spans Lithuania, Latvia, and Estonia and hosts numerous onshore and offshore hydrocarbon and deep saline reservoirs, mainly composed of sandstone and carbonate formations [2,5–8]. These reservoirs, along with over 50 depleted oil and gas fields, present viable options for permanent and safe CO_2 storage. The reservoirs assessed for CO_2 storage can also be utilized for Hydrogen storage [9,10]. However, to effectively utilize these reservoirs for Hydrogen storage, a deeper understanding of its behavior in the subsurface is required, particularly related to flow and migration behavior, geochemical and geomechanical interactions, trapping mechanisms, leakage risks and caprock integrity, as such studies are limited and often utilize models developed for CO_2 or natural gas, leading to high uncertainty for Hydrogen storage [11–13].

Researchers have conducted numerical simulations to understand the flow behavior of CO_2 in subsurface reservoirs. Wen and Benson [14] used TOUGH2 to understand the impact of layering and vertical heterogeneity on plume shape, migration, and dissolution rate, observing that layering changes the plume footprint and moderate heterogeneity increases dissolution. Wang et al. [15] used the finite volume method (FVM) in the MRST toolbox to study the impact of reservoir properties on CO_2 storage, focusing on the migration process and storage capacity of a saline aquifer. They observed that depth and permeability play key roles in plume migration and storage capacity, and that dissolution and mineralization become important mechanisms for long-term storage of CO_2. A similar study by Wang et al. [16] examined the injectivity and migration behavior of CO_2 for different well types (horizontal and vertical) in a saline aquifer in China, highlighting that horizontal wells enhance injection volume compared to vertical wells.

Although most studies focus on CO_2 storage, these modeling approaches are often extended to investigate Hydrogen storage, including cases where CO_2 is used as a cushion gas, even though Hydrogen has different physical properties and migration behavior. Wang et al. [17] performed a 2D numerical simulation to examine Hydrogen storage using CO_2 as a cushion gas, observing that less viscous Hydrogen leaves CO_2 behind in some regions, reducing Hydrogen purity. Additionally, if CO_2 solubility is considered, it tends to improve Hydrogen purity, and in gravity-dominated regimes, Hydrogen accumulates at the top, displacing CO_2. Ren et al. [18] compared buoyant flows of Hydrogen and CO_2 by focusing on density, viscosity, and relative permeability, showing that Hydrogen produces a more pronounced upward migration and channeling risk than CO_2. Core-scale sandstone experiments using low-field nuclear magnetic resonance (NMR) showed that Hydrogen mainly occupies large pores, with low residual saturation and slightly improved recovery over cycles, indicating favorable behavior for underground Hydrogen storage (UHS) [19]. These results emphasize that screening criteria for Hydrogen need to weigh in parameters differently than for CO_2.

Geochemical studies further highlight the interaction of CO_2 and Hydrogen with reservoir rocks and brine upon injection. The coreflooding experiments for CO_2 injection show the dissolution and precipitation of different minerals [20–25], while Hydrogen exposure has been shown to affect mineral composition and elastic properties in sandstone [26,27]. For UHS, one key requirement is the recovery of Hydrogen at the time of need, and injection can lead to interactions with the formation rock and brine, affecting recovery. These findings suggest that Hydrogen does not appear to pose a risk of loss and reservoir integrity due to the geochemical mechanism alone. In addition, long-term storage safety also depends on wellbore integrity, which is critical for preventing leakage along injection wells. A recent study by Vytyaz et al. [28] demonstrates that tailored cement compositions and polycomponent plugging systems can improve well sealing under complex

operating conditions. Integrating wellbore assessments with geomechanical evaluations of the reservoir allows a more comprehensive evaluation of storage safety, including risks of unintended migration, geochemical alterations, pressure-induced fracturing, and leakage.

This study addresses these gaps by evaluating CO_2 and Hydrogen injection under identical reservoir conditions, integrating numerical modeling with laboratory experiments to provide a unified assessment of flow dynamics, geomechanical stability, and geochemical alterations, including mineral precipitation and dissolution in saline aquifers. Using the workflow presented in Malik et al. [7], a field-scale reservoir simulation model is developed to assess CO_2 flow behavior and subsequently extended to investigate Hydrogen flow behavior in the Lithuanian saline aquifer, Syderiai. This study will provide, for the first time, a comparative and detailed numerical assessment of CO_2 and Hydrogen flow behavior and storage potential in the Syderiai saline aquifer. Additionally, experiments on the geochemical impact of CO_2 and Hydrogen on rock and formation brine are presented. The results establish a foundation for future CCUS and Hydrogen project development in the Baltic Basin, offering critical insights for policymakers, industry stakeholders, and researchers seeking to advance carbon-mitigation technologies in the region.

The paper is organized as follows: an introduction to research on migration mechanisms, geomechanical response, and geochemical studies is presented in Section 1. This is followed by Section 2, which describes the study area and provides details of rock samples and laboratory measurements. Section 3 presents the methodology adopted for both numerical simulation and experimental studies. Section 4 presents the simulation and experimental results for both CO_2 and Hydrogen. Section 5 presents a comparative analysis of the results obtained. Finally, the study is concluded in Section 6

2. Geological Setting and Laboratory Measurements

2.1. Geological Setting

In this study, we will primarily focus on the Syderiai saline aquifer of Lithuania. The saline aquifers are among the most promising candidates for geological CO_2 storage, alongside depleted hydrocarbon reservoirs, due to their wide availability and suitable properties. The preliminary investigation by Malik et al. [7] showed that the Syderiai aquifer has a CO_2 storage potential of 54–232 Mt after 30 years of injection. The reservoir can also be a good target for storing Hydrogen. The Syderiai saline aquifer is located in western Lithuania and comprises sandstones from the Middle Cambrian Deimena series. The aquifer has a porosity of 16% and a permeability of 400 mD. The total area of the Syderiai aquifer is estimated to be around 26 km^2, with a thickness of 57 m and a top depth of 1458 m [5,8].

In this study, we aim to investigate the CO_2 and Hydrogen plume migration behavior in the Syderiai saline aquifer. The average reservoir properties of this saline aquifer are summarized in Table 1 and serve as the basis for subsequent numerical simulations.

2.2. Laboratory Measurements

The experiments are performed on two outcrop samples representative of the Syderiai saline aquifer in Lithuania in terms of petrophysical properties, such as porosity and permeability, and mineralogical composition. The properties of the rock samples used in the experiment are described in Table 2. The rock samples are scanned using Scanning Electron Microscopy (SEM), and their X-ray diffraction patterns are obtained both before and after the experiments to assess the impact of fluid (CO_2 and Hydrogen) injection on rock properties. The different measurement methods adopted are described in the following subsection.

Table 1. Average properties of the Syderiai saline aquifer in Lithuania.

Properties	Values
Stratigraphic Unit	Middle Cambrian
Formation	Deimena
Lithology	Sandstone
Total Area (sq. km)	26
Top Depth (m)	1458
Porosity (%)	16
Permeability (mD)	400
Thickness (m)	57
NTG	0.75

Table 2. Properties of the outcrop core samples used in laboratory experiments.

Properties	BB Sample	BS Sample
Porosity (%)	21.60	20.28
Permeability (mD)	242.58	39.79

2.2.1. X-Ray Diffraction (XRD)

XRD measurements are performed using a Malvern Panalytical EMPYREAN Series 3 (Malvern, Worcestershire, UK) diffractometer equipped with a Cu tube and 1DER detector. Clay fractions (<0.2 µm and <2 µm) are separated using standard Jackson techniques and are Na+ saturated prior to analysis. Measurements were performed on sedimented slides (5 mg/cm^2) scanned from 2° to 50° 2Θ with a step size of 0.02°, under both air-dried and glycolated conditions, at 40 kV and 40 mA. The interpretation of the diffraction pattern followed the methodology of Moore and Reynolds [29] and Środoń [30], applying the NEWMOD program [31] to determine the proportion and ordering degree of illite–smectite mixed layers. The XRD measurements performed before the experiment are shown in Figure 1.

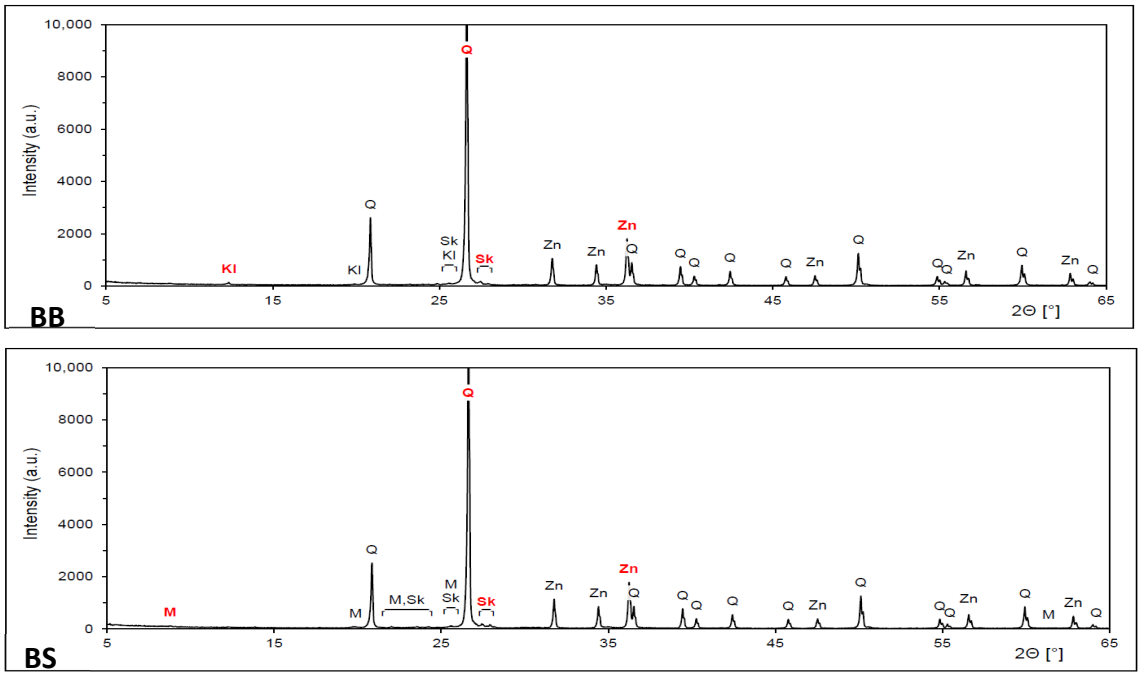

Figure 1. XRD plots for the BB and BS samples obtained before conducting the experiments. Q: Quartz, Kl: Kaolinite, Sk: Potassium feldspar, M: Mica and Illite.

Figure 1 shows the peaks of minerals identified from the XRD pattern. The position, intensity, and shape of these peaks allow the identification and quantification of the specific crystalline minerals.

2.2.2. Scanning Electron Microscopy (SEM)

The SEM imaging is performed using a JEOL JSM-6300 SEM (Tokyo, Japan) equipped with an energy-dispersive X-ray spectroscopy (EDS) microprobe. Analyses are performed at accelerating voltages of 5–30 kV to obtain high-resolution images and elemental maps of the rock matrix, cement, and pore spaces. Prior to imaging, the samples are polished and coated with a thin platinum layer to ensure electrical conductivity during electron-beam exposure. The EDS system enabled point and area chemical analyses for identifying mineral phases and their spatial distribution. Platinum peaks observed in the EDS spectra are attributed to the coating and excluded from interpretation.

3. Methodology

The present work is divided into two parts: the first is the simulation part to study the plume migration of both CO_2 and Hydrogen and its impact on different properties such as pressure, pH, gas saturation, and geomechanical properties, and the second part is the experimental study focusing on rock-brine-fluid (CO_2 and Hydrogen) interaction.

3.1. Simulation Methodology

A compositional reservoir simulation is conducted to investigate the migration mechanisms of CO_2 and Hydrogen during injection into a deep saline aquifer. The study employed a three-dimensional Cartesian model of a confined aquifer system with heterogeneous formations and no-flow boundaries on all sides to extract a two-dimensional slice. The 3D model is based on the Syderiai box model (see Figure 2), which represents a simplified conceptualization of the reservoir using average petrophysical properties such as porosity and permeability. The approach is often categorized as a mechanistic modeling approach, see details in [7]. The properties used in this model are taken from [7]. This approach provides a practical framework for understanding plume dynamics while maintaining computational efficiency.

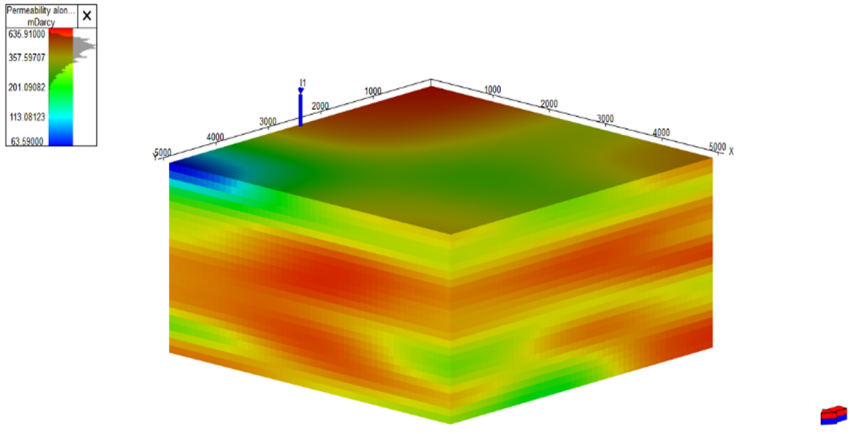

Figure 2. Syderiai saline aquifer box model, showing permeability distribution along X axis.

The 2D slice extracted from the 3D model is used in the present study to analyze and visualize the movement of the CO_2 and Hydrogen plumes (see Figure 3 showing permeability and porosity distribution) during and after injection. The present simulation model has one cell in the x-direction, 50 in the y-direction, and 25 in the z-direction (see Table 3). The grid resolution is selected to ensure adequate vertical and lateral representation of CO_2

and Hydrogen plume development, with additional refinement near the injection region to capture fine-scale multiphase flow behavior, as shown in Figure 4.

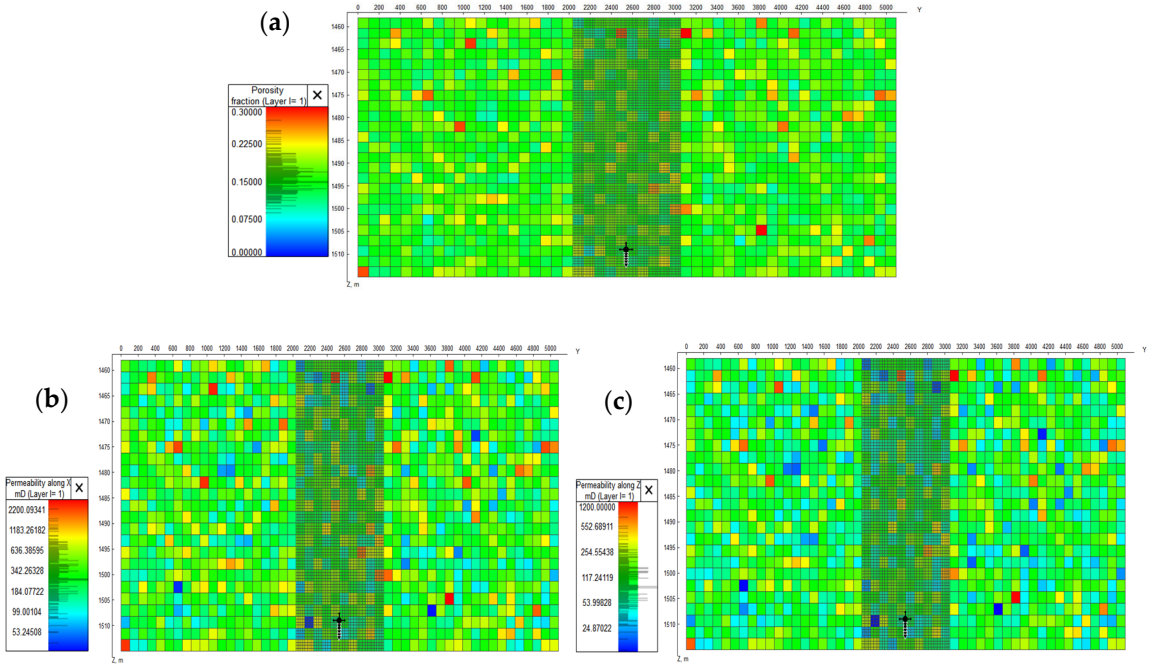

Figure 3. (**a**) Porosity distribution, (**b**) Permeability distribution along X axis, and (**c**) Permeability distribution along Z axis, plot. The '✝' symbol indicates the injection well.

Table 3. Grid dimensions used in the mechanistic model.

Parameters	Dx (m)	Dy (m)	Dz (m)	Nx	Ny	Nz
Values	101.9	101.9	2.28	1	50	25

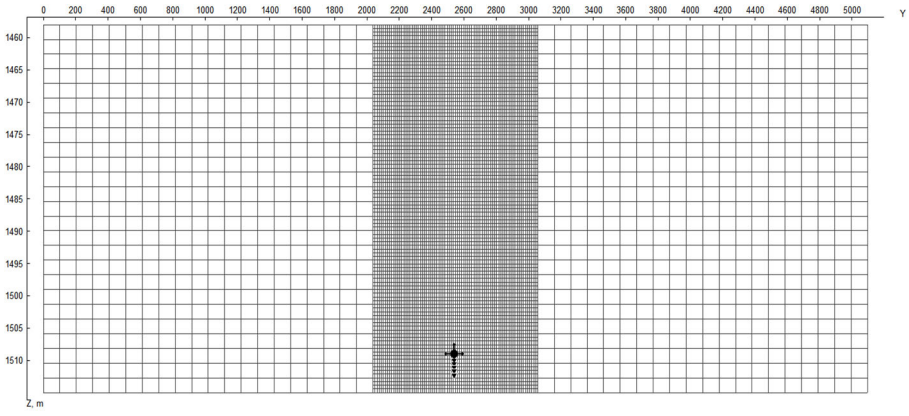

Figure 4. Grid refinement applied to the model with refinement factor in X-direction, Y-direction: 5 times (Layer 21–30), and Z-direction: 4 times (Layer 1–25). The '✝' symbol indicates the injection well.

A single vertical injection well is placed at the center of the refined region, perforating from the 23rd to the 24th layer of the aquifer, as shown in Figure 4. The well is operated under bottom-hole pressure (BHP) control, with an upper pressure limit of 450 bar, and an injection rate of 11,000 standard cubic meters per day. These BHP and injection rate assumptions are based on the CO_2 field injection trial conducted by UAB Minijos Nafta, in which 1000 tons of CO_2 were injected per day into the Gargzdai hydrocarbon reservoir [32]. To explore sensitivity to lower injectivity scenarios and provide a conservative low-case assessment, an additional simulation case with a reduced injection rate of 5000 standard

cubic meters per day is also considered. The injection continued until the target reservoir pressure was achieved, or for a maximum of 5 years, after which the system was allowed to evolve under shut-in conditions to simulate post-injection migration.

The injection period is followed by a five-year extended monitoring period to evaluate pressure dissipation, plume stabilization, and the extent of CO_2 dissolution into the formation water. The properties used in the simulation are listed in Table 4. The simulations are performed using a commercial reservoir simulator, tNavigator (version 25.2) [33], and the keyword GASSOL is used to enable gas solubility in the water phase. Additionally, no flow boundary conditions are assumed.

Table 4. Reservoir properties used in the mechanistic simulation model.

Properties	Values
Porosity (%)	16
Permeability X (mD)	400
Permeability Y (mD)	400
Permeability Z (mD)	133
Thickness (m)	57
NTG	0.75
Salinity (g/L)	122
Aquifer Pressure (bars)	153
Young's modulus (bars) [34]	350,000
Poisson's ratio	0.2
Bottom Hole Pressure (bars)	450
Injection rate	5000 and 11,000 Sm^3/day
Injection period	5 years
Monitoring period	5 years

Geomechanical Study: The flow behavior simulation is followed by a coupled geomechanical flow simulation to study the impact of CO_2 and Hydrogen injection on reservoir integrity. The injection is performed for 5 years, followed by a 5-year monitoring period. The properties utilized in the simulation are given in Table 4. Once the properties are assigned to the model, the GEOMECH keyword option in tNavigator is used. In GEOMECH, the FE option is specified, which defines a fully coupled approach: at each step of the simulator, a joint system of coupled equations describing the fluid flow processes in the reservoir and the geomechanical effects is solved using the finite element method (FEM) for rock stress calculation [33]. In addition, rigid boundary conditions are assumed with zero displacement set at all model faces. Vertical stress is measured to assess the mechanical stability of reservoirs under injection.

3.2. Experimental Methodology

The flooding experiments are carried out for both CO_2 and Hydrogen using outcrop samples representative of the Syderiai saline aquifer. Similar to the Syderiai aquifer, the sandstone outcrop samples are quartz-dominant, with minor clay minerals, and exhibit porosity and permeability values representative of aquifer properties, reflecting the heterogeneity of the formation. The rock samples are analyzed after the experiments to observe rock–brine–fluid interactions that result in mineralogical changes, such as precipitation and dissolution.

CO_2 flooding experiment: The rock sample is first saturated with brine salinity of the Syderiai aquifer (122 g/L) under vacuum. The sample is then placed in a coreflooding apparatus, where cyclic brine injection (brine-CO_2-brine) is performed to study the impact of CO_2 injection on rock properties. Liquid CO_2 is injected into the rock samples in the

experiment. The SEM images of the samples are obtained and analyzed for mineralogical changes [24,25].

Hydrogen flooding experiment: Rock samples are prepared for SEM image analysis, and images are obtained before the experiment, along with XRD measurements. The prepared rock sample is then placed in an autoclave for aging in Hydrogen under reservoir pressure (150 bar) and temperature conditions (BB—33 °C; BS—50 °C). The sample is kept in the autoclave for 4 months, after which SEM images are acquired again, along with XRD measurements, to observe changes in rock mineralogy.

The experiments are performed to complement the simulation results by confirming rock-specific reactions that are not fully captured in the model, thereby enhancing understanding of rock–brine–fluid interactions.

4. Results

The section is divided into two parts. First, the simulation results for both CO_2 and Hydrogen injection are presented. Then, in the second part, the experimental results are presented.

4.1. Simulation Results

The flow simulation is performed for CO_2 and Hydrogen at two injection rates, 5000 and 11,000 Sm^3/day, with a 5-year injection period followed by a 5-year monitoring period. The changes in pH level, gas saturation, and pressure distribution are first measured to understand the flow behavior of both CO_2 and Hydrogen. This is followed by observing changes in stress over the 10 years to examine the geomechanical impact of injection on the integrity of the formation reservoir. The results are discussed in the following sections.

4.1.1. CO_2 Injection

Pressure Variation: Figures 5 and 6 show pressure changes over 10 years, with a 5-year injection period and a 5-year monitoring period, for injection rates of 5000 Sm^3/day and 11,000 Sm^3/day, respectively. In both cases, the pressure gradually increases as more CO_2 is added to the formation. The injected CO_2 occupies the pore space, displacing brine, and, as the system is closed, the displaced brine remains within the formation, causing a pore pressure buildup. Additionally, it interacts with brine and dissolves in it. This partial dissolution mitigates further increases in pressure. The pressure reaches a maximum of 203 bar at an injection rate of 5000 Sm^3/day, whereas it reaches 274 bar at an injection rate of 11,000 Sm^3/day near the injection well by the end of the injection period. Once the well is shut, the maximum pressure decreases slightly as the plume spreads and equilibrates during the 5-year monitoring period.

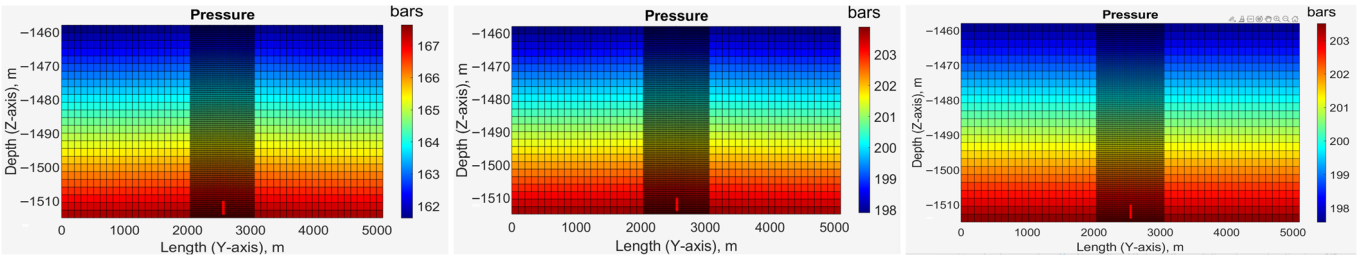

Figure 5. Pressure evolution after injecting CO_2 at 5000 Sm^3/day for 5 years, followed by a 5-year observation period from 153 bar to 203 bar (**left**: 1 year, **middle**: 5 years, **right**: 10 years).

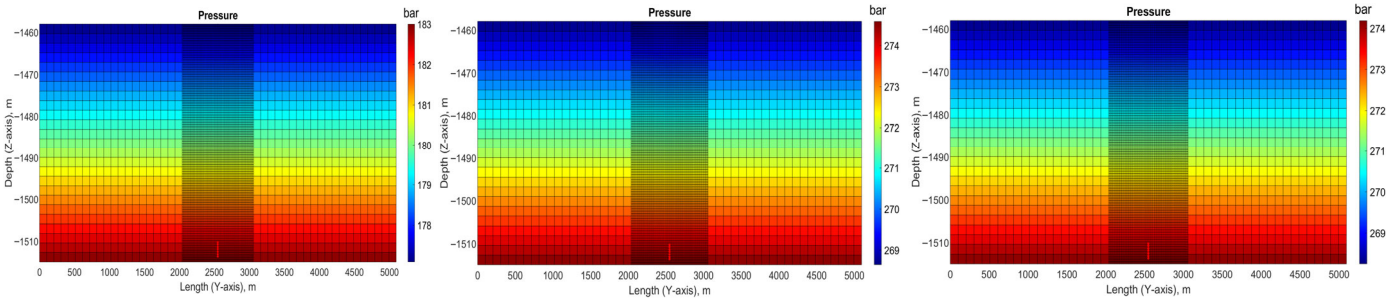

Figure 6. Pressure evolution after injecting CO_2 at 11,000 Sm^3/day for 5 years, followed by a 5-year observation period from 153 bars to 274 bars (**left**: 1 year, **middle**: 5 years, **right**: 10 years).

Gas saturation variation: Figures 7 and 8 show the evolution of gas saturation in the aquifer after injecting CO_2 for 5 years, followed by monitoring for the next 5 years at injection rates of 5000 Sm^3/day and 11,000 Sm^3/day, respectively. In both cases, when CO_2 is injected, it rises towards the top of the formation due to its lower density than brine, and the plume size increases as injection continues. Once the injection stops, the plume starts spreading laterally at the top of the formation over the 5-year monitoring period. The plume shown in Figure 7 is comparatively narrower, with reduced vertical thickness and lateral extent, than that shown in Figure 8, due to a lower injection rate resulting in a lower injected volume.

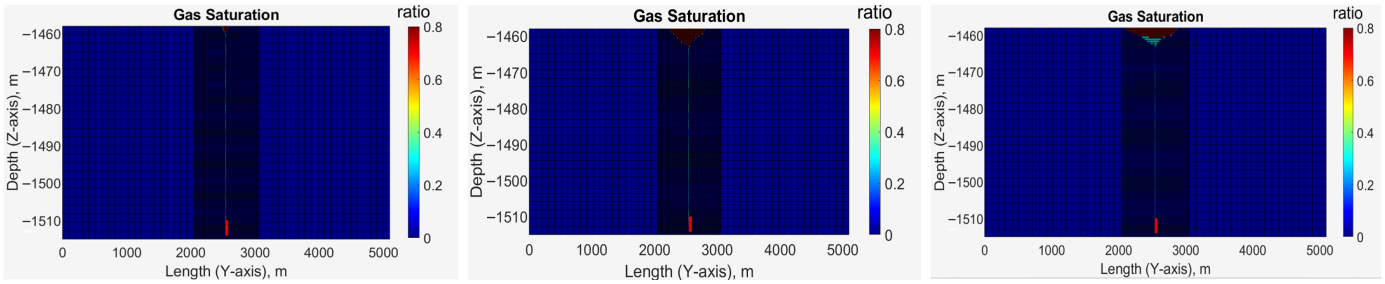

Figure 7. Gas saturation evolution after injecting CO_2 for 5 years, followed by a 5-year observation period at 5000 Sm^3/day injection rate (**left**: 1 year, **middle**: 5 years, **right**: 10 years).

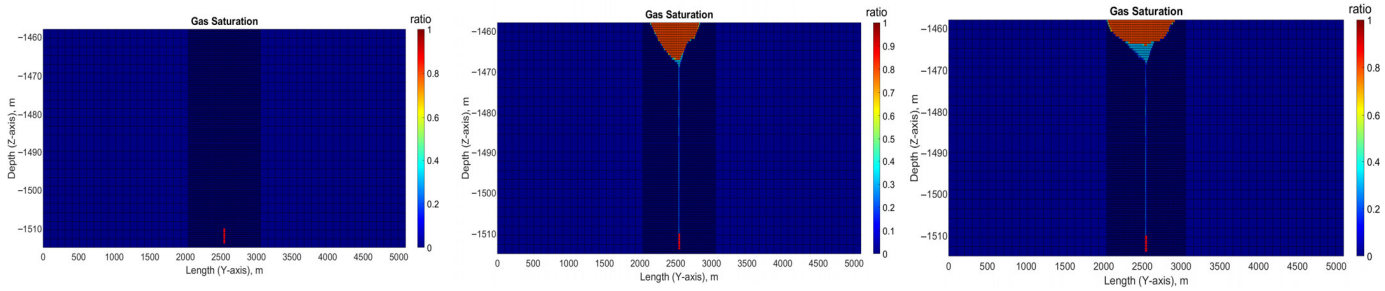

Figure 8. Gas saturation evolution after injecting CO_2 for 5 years, followed by a 5-year observation period at 11,000 Sm^3/day injection rate (**left**: 1 year, **middle**: 5 years, **right**: 10 years).

pH variation: Figures 9 and 10 show the 2D cross-sections of pH evolution in the aquifer after 5 years of injecting CO_2 at 5000 Sm^3/day and 11,000 Sm^3/day, respectively, followed by 5 years of observation. In both cases, as CO_2 is injected, it starts dissolving into brine near the well in layers 23–24, forming carbonic acid (H_2CO_3) and lowering pH in a localized zone around the injection well. As CO_2 continues to migrate towards the top of the formation, it interacts with the brine, reducing the pH and indicating progressive chemical alteration potential within the formation. The pH of the formation drops from 6.8 to 4.4,

making it acidic. This low-pH region extends both laterally and vertically, showing a more pronounced effect.

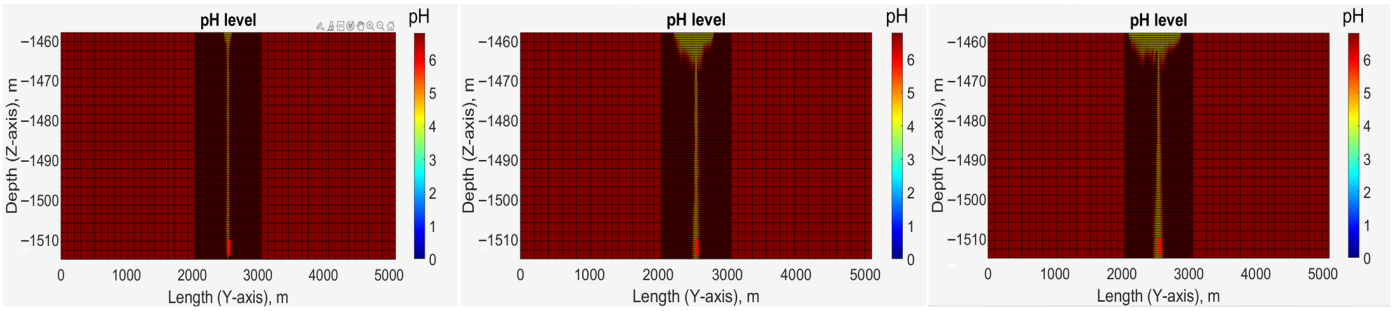

Figure 9. pH evolution after injecting CO_2 at 5000 Sm^3/day for 5 years, followed by a 5-year observation period (**left**: 1 year, **middle**: 5 years, **right**: 10 years).

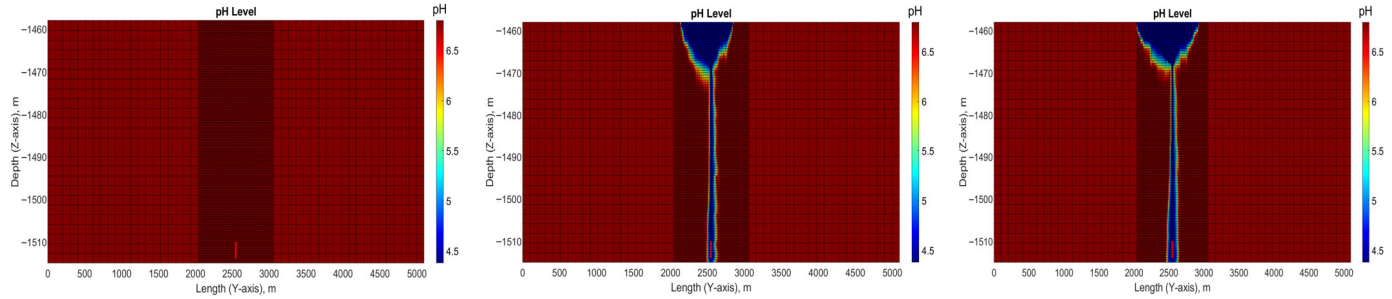

Figure 10. pH evolution after injecting CO_2 at 11,000 Sm^3/day for 5 years, followed by a 5-year observation period (**left**: 1 year, **middle**: 5 years, **right**: 10 years).

Additionally, pH fingers are observed in Figures 9 and 10 towards the end of the simulation due to the dissolution of CO_2 into the brine, forming CO_2-saturated brine that is denser than the formation brine. This denser, acidic brine sinks slightly under gravity, creating downward-protruding fingers via density-driven convection and viscous instability at the interface between the CO_2-rich brine and the formation brine. No significant pH recovery occurs because dissolved CO_2 remains trapped in solution, indicating long-term geochemical alteration confined to the plume footprint after 10 years.

Geomechanical Impact: Once the CO_2 flow behavior is observed, a coupled geomechanical simulation is conducted to assess the impact of injection-induced overpressure on reservoir mechanical integrity. It is observed that, as CO_2 is injected, the vertical stress gradually increases across the reservoir (Figures 11 and 12) due to poroelastic coupling with rising pore pressure. At an injection rate of 5000 Sm^3/day (Figure 11), it reaches a maximum of 286 bars, reflecting lower pore pressure buildup from a smaller injected volume, whereas it reaches a maximum of 423 bars near the injection well by the end of the injection period at 11,000 Sm^3/day (Figure 12).

During the subsequent 5-year post-injection monitoring period, vertical stress decreased slightly due to CO_2 solubility in brine, reflecting a stable mechanical system transitioning toward equilibrium. This study demonstrates the geomechanical response under more conservative injectivity scenarios and the rate-dependent stress evolution.

4.1.2. Hydrogen Injection

Pressure Variation: Figures 13 and 14 show the pressure evolution from the start of injection to the end of the monitoring period (10 years) for injection rates of 5000 Sm^3/day and 11,000 Sm^3/day, respectively. It is observed that as Hydrogen injection begins, the reservoir pressure increases, reaching 256 bars at 5000 Sm^3/day injection rate and 329 bars

at 11,000 Sm^3/day injection rate near the injection well by the end of the 5-year injection period. The increase in both cases during the injection period is due to the addition of significant mass to the closed system. This increase in pressure is greater than that observed during CO_2 injection, because Hydrogen, being highly compressible and very poorly soluble in brine, remains almost entirely in the free phase, occupying pore space and raising pore pressure rather than dissolving into the formation fluid. Once the well is shut, the reservoir pressure remains almost constant for the next 5 years, i.e., the monitoring period.

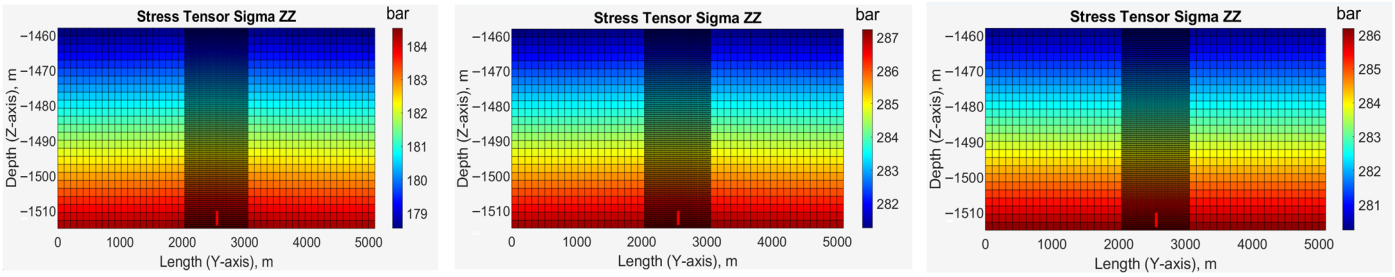

Figure 11. Vertical stress evolution after injecting CO_2 at 5000 Sm^3/day for 5 years, followed by a 5-year observation period, reaching a maximum value of 286 bars (**left**: 1 year, **middle**: 5 years, **right**: 10 years).

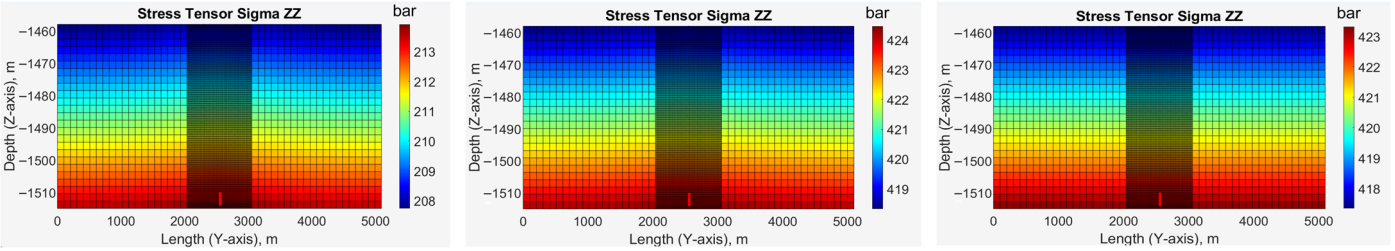

Figure 12. Vertical stress evolution after injecting CO_2 at 11,000 Sm^3/day for 5 years, followed by a 5-year observation period, reaching a maximum value of 423 bars (**left**: 1 year, **middle**: 5 years, **right**: 10 years).

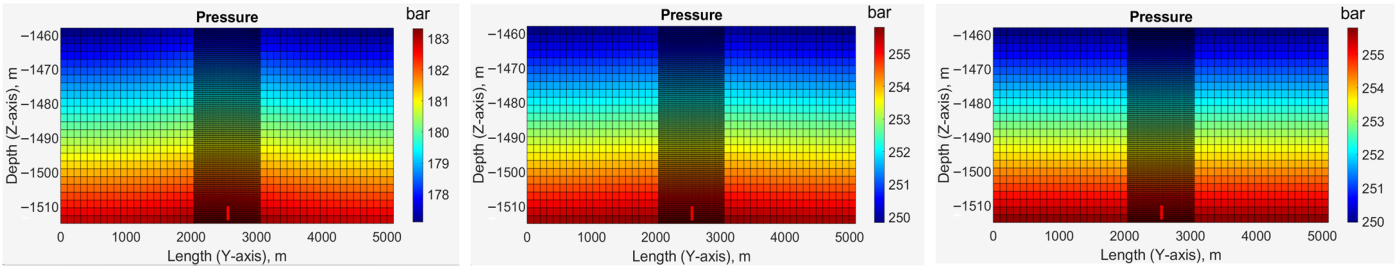

Figure 13. Pressure evolution after injecting Hydrogen at 5000 Sm^3/day for 5 years, followed by a 5-year observation period (**left**: 1 year, **middle**: 5 years, **right**: 10 years).

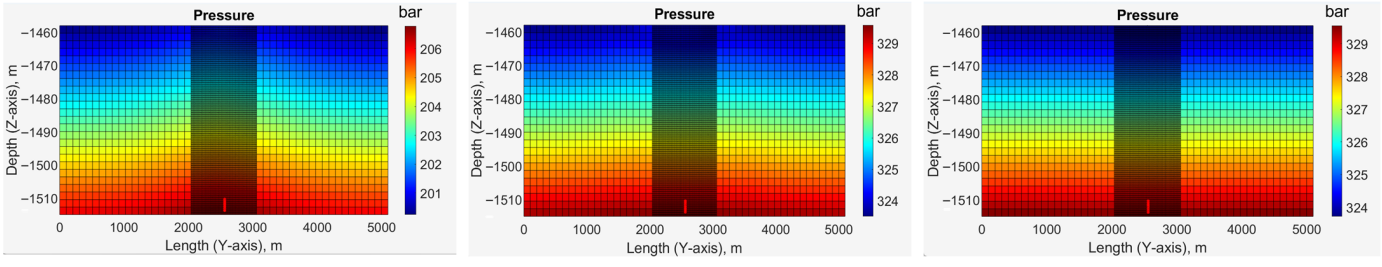

Figure 14. Pressure evolution after injecting Hydrogen at 11,000 Sm^3/day for 5 years, followed by a 5-year observation period (**left**: 1 year, **middle**: 5 years, **right**: 10 years).

Gas saturation variation: Figures 15 and 16 show the gas saturation evolution after 5 years of Hydrogen injection at 5000 Sm^3/day and 11,000 Sm^3/day, respectively, followed by a 5-year monitoring period. In both cases, as injection begins, Hydrogen starts rising to the top of the reservoir and accumulates there due to its extreme buoyancy (low density compared to the formation brine) and low viscosity. It forms a thin, high-saturation gas cap at the caprock-formation interface with no vertical movement or fingering occurring at any time. As the injection continues, the plume thickness increases slightly while spreading laterally. Once the well is shut, the gas continues to spread laterally, with maximum saturation at the top of the reservoir. In the lower injection rate case, the total injected volume is lower, resulting in a thinner gas cap with reduced vertical thickness and lateral extent compared to the higher injection rate case.

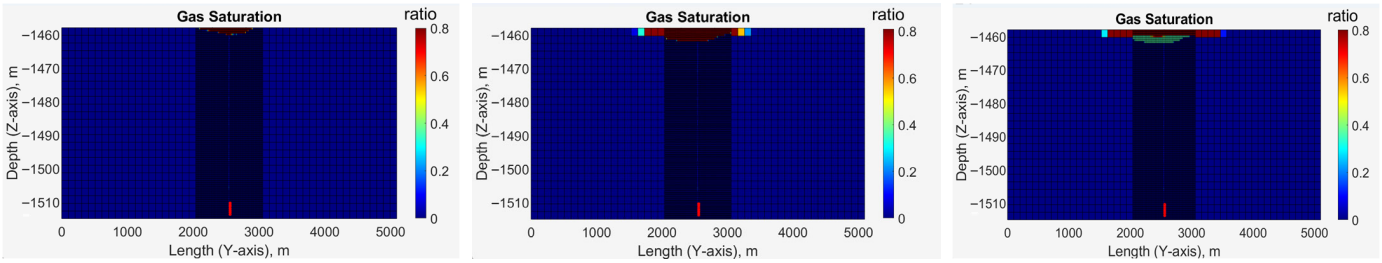

Figure 15. Gas saturation evolution after injecting Hydrogen at 5000 Sm^3/day for 5 years, followed by a 5-year observation period (**left**: 1 year, **middle**: 5 years, **right**: 10 years).

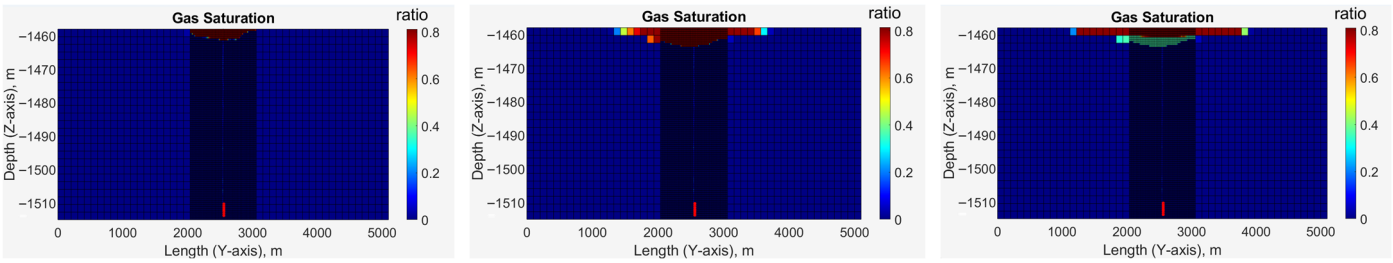

Figure 16. Gas saturation evolution after injecting Hydrogen at 11,000 Sm^3/day for 5 years, followed by a 5-year observation period (**left**: 1 year, **middle**: 5 years, **right**: 10 years).

pH variation: In the Hydrogen injection simulations, the pH evolution after 5 years (Figures 17 and 18) of injection, followed by a 5-year monitoring period for both the injection rates (5000 Sm^3/day and 11,000 Sm^3/day), reveals that, unlike CO_2 injection, the pH of the formation brine remains relatively unchanged over time. The pH distribution shows almost no deviation from the formation pH, indicating that Hydrogen, being a nonreactive, weakly soluble gas under reservoir conditions, does not undergo significant chemical interaction with the brine. The uniformity of pH across the reservoir in both cases suggests that even prolonged Hydrogen exposure does not lead to notable interaction with the brine.

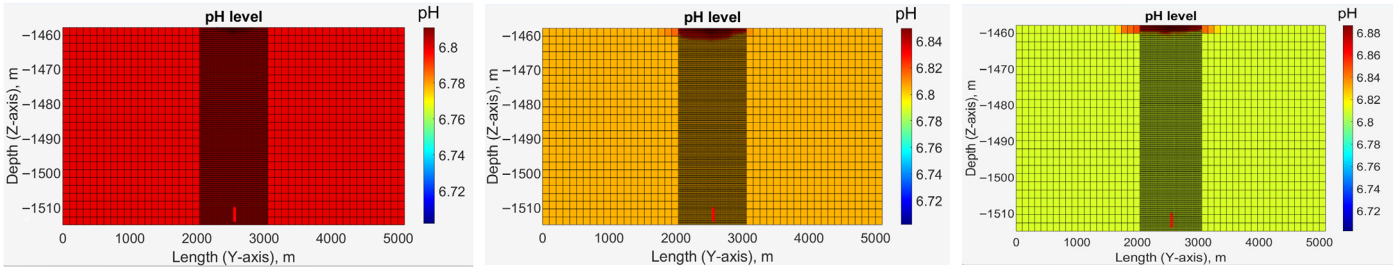

Figure 17. pH evolution after injecting Hydrogen at 5000 Sm^3/day for 5 years, followed by a 5-year observation period (**left**: 1 year, **middle**: 5 years, **right**: 10 years).

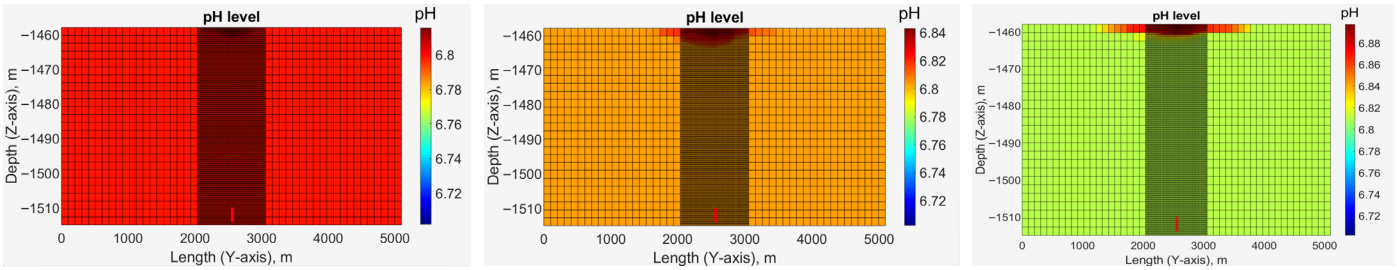

Figure 18. pH evolution after injecting Hydrogen at 11,000 Sm^3/day for 5 years, followed by a 5-year observation period (**left**: 1 year, **middle**: 5 years, **right**: 10 years).

Geomechanical Impact: Similar to CO_2, a coupled geomechanical flow simulation is conducted for Hydrogen injection to assess its impact on reservoir integrity over the 10 years. It is observed that the vertical stress (shown in Figure 19) increases rapidly to 380 bars at an injection rate of 5000 Sm^3/day and to the maximum value of 450 bars at 11,000 Sm^3/day (Figure 20) injection rate near the injection well region, leading to the shutting of the well within 4 years of injection due to the BHP limit. The stress then remains constant till the end of the simulation. The rapid rise in vertical stress is due to continuous Hydrogen injection in a confined system, which increases pore pressure. Because Hydrogen has extremely low solubility in brine, nearly the entire injected mass remains as free gas, occupying pore space and displacing brine without significant pressure relief through dissolution.

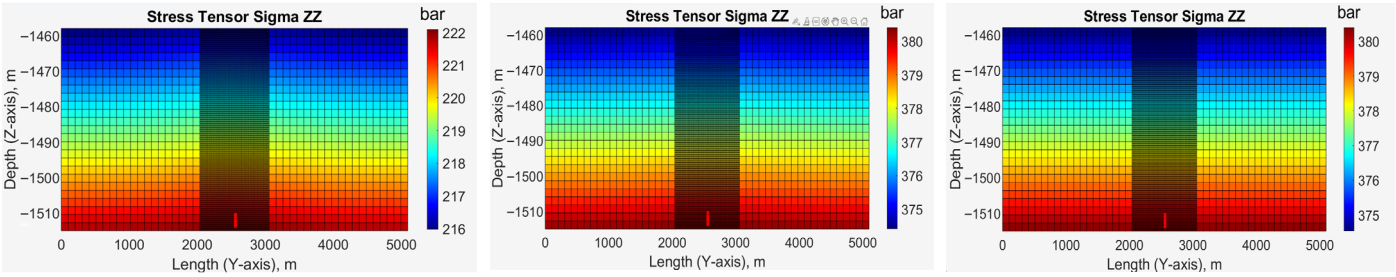

Figure 19. Vertical stress tensor evolution after injecting Hydrogen at 5000 Sm^3/day for 5 years, followed by a 5-year observation period, reaching a maximum value of 380 bars (**left**: 1 year, **middle**: 5 years, **right**: 10 years).

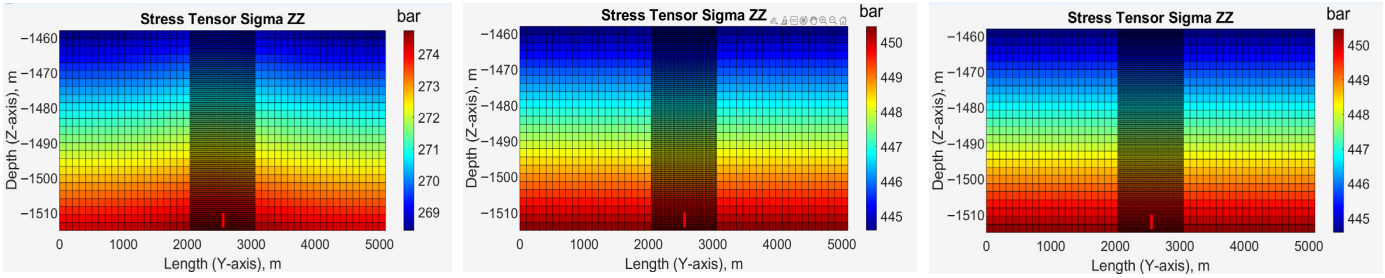

Figure 20. Vertical stress tensor evolution after injecting Hydrogen at 11,000 Sm^3/day for 5 years, followed by a 5-year observation period, reaching a maximum value of 450 bars (**left**: 1 year, **middle**: 5 years, **right**: 10 years).

This rate sensitivity highlights a stronger geomechanical response to Hydrogen than to CO_2, primarily because of its lack of solubility trapping.

The numerical simulations provide a detailed understanding of the fluid flow behavior, geochemical interactions in terms of pH changes, and the geomechanical response of the reservoir during CO_2 and Hydrogen injection. While the simulations capture pressure

evolution, gas migration, pH trends, and stress changes, the mineral-scale reactions represented in the models remain generalized and rely on thermodynamic databases rather than direct observation. To further understand the chemical changes predicted in the simulation—especially the pH-driven reactions during CO_2 injection and the subtle but non-negligible effects during Hydrogen exposure—experimental work was conducted.

4.2. Experimental Results

The outcrop samples are exposed to CO_2 and Hydrogen via coreflooding and autoclave aging, respectively, to observe variations in the mineralogy of the samples due to rock–brine–fluid (CO_2 and Hydrogen) interactions. XRD and SEM analyses are performed to observe changes.

4.2.1. CO_2 Flooding Results

SEM images were acquired before and after the coreflooding experiment from different locations within the samples. The SEM image analysis shows precipitation of halite minerals after exposure to CO_2, as shown in Figure 21. The results are discussed in [24,25]. In addition, the effluent collected during the experiment showed a drop in pH compared to the pre-experimental values.

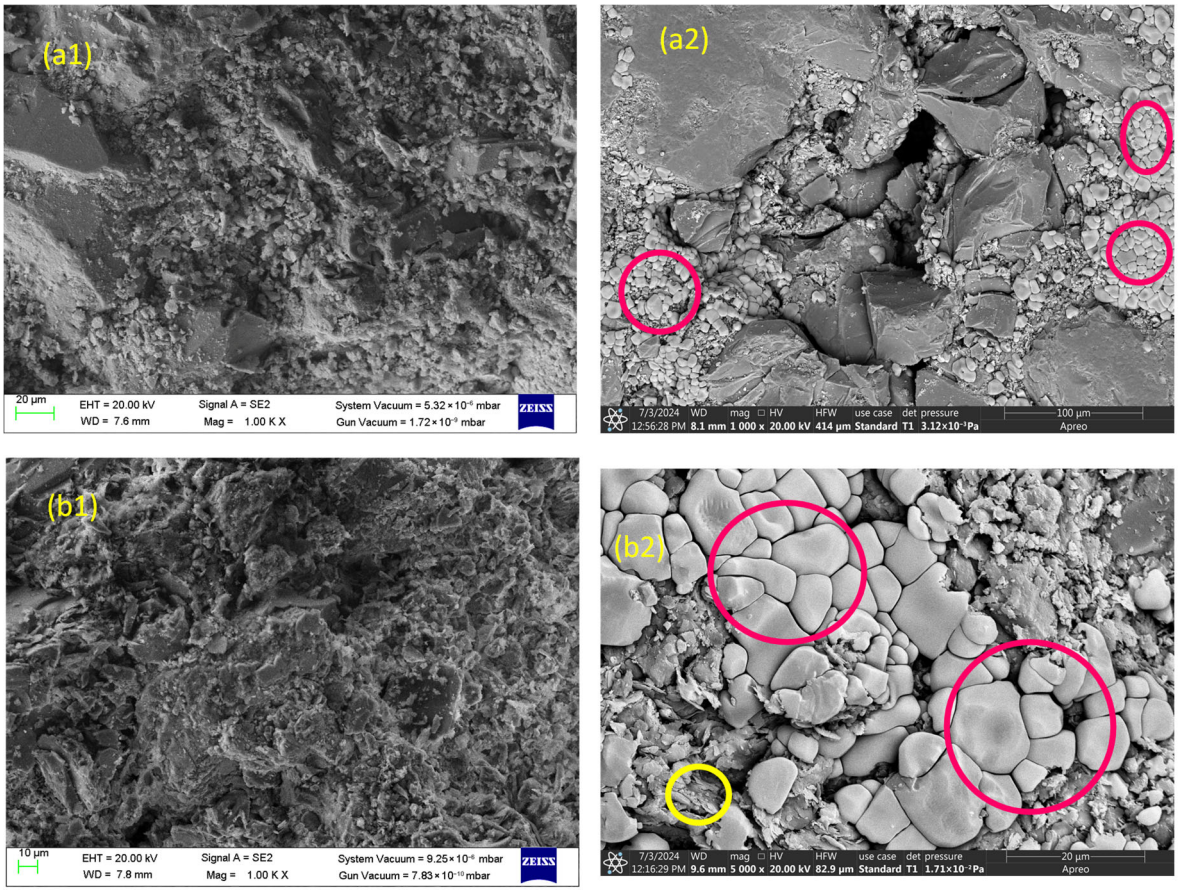

Figure 21. SEM images obtained before (**a1**,**b1**) and after the CO_2 coreflooding experiment (**a2**,**b2**), showing the precipitation of halite (pink circle) and illite minerals (yellow circle). Here, (**a1**,**a2**) are images of the BB sample and (**b1**,**b2**) are images of the BS sample.

The mineralogical changes observed are analyzed using XRD measurements, as shown in Table 5. It can be seen that precipitation of halite has occurred in both samples, with dissolution of feldspar, plagioclase, and kaolinite in the BB sample, and dissolution of quartz, plagioclase, feldspar, mica, and illite in the other sample (BS).

Table 5. Comparison of the quantitative analyses of mineral composition obtained using the XRD method for the BB and BS samples, before and after the CO_2 flooding experiment.

Sample	Before Experiment	After Experiment
BB	Quartz 80.1% Plagioclase 3.3% Potassium Feldspar 9.3% Kaolinite 7.3%	Quartz 82.1% Plagioclase 0.5% Potassium Feldspar 8.0% Kaolinite 5.1% Halite 1.7% Mica + Illite 2.6%
BS	Quartz 76% Plagioclase 4.3% Potassium Feldspar 7.6% Mica + Illite 12.1%	Quartz 74.5% Plagioclase 7.6% Potassium Feldspar 10.9% Mica + Illite 5.5% Halite 1.5%

4.2.2. Hydrogen Aging Results

After aging the rock samples in Hydrogen in an autoclave for four months, SEM images were acquired and compared with pre-experiment images. In addition to halite precipitation shown in Figure 22, dissolution of feldspars and iron hydroxides, dissolution and recrystallization of quartz, and calcitization of glauconite are also observed.

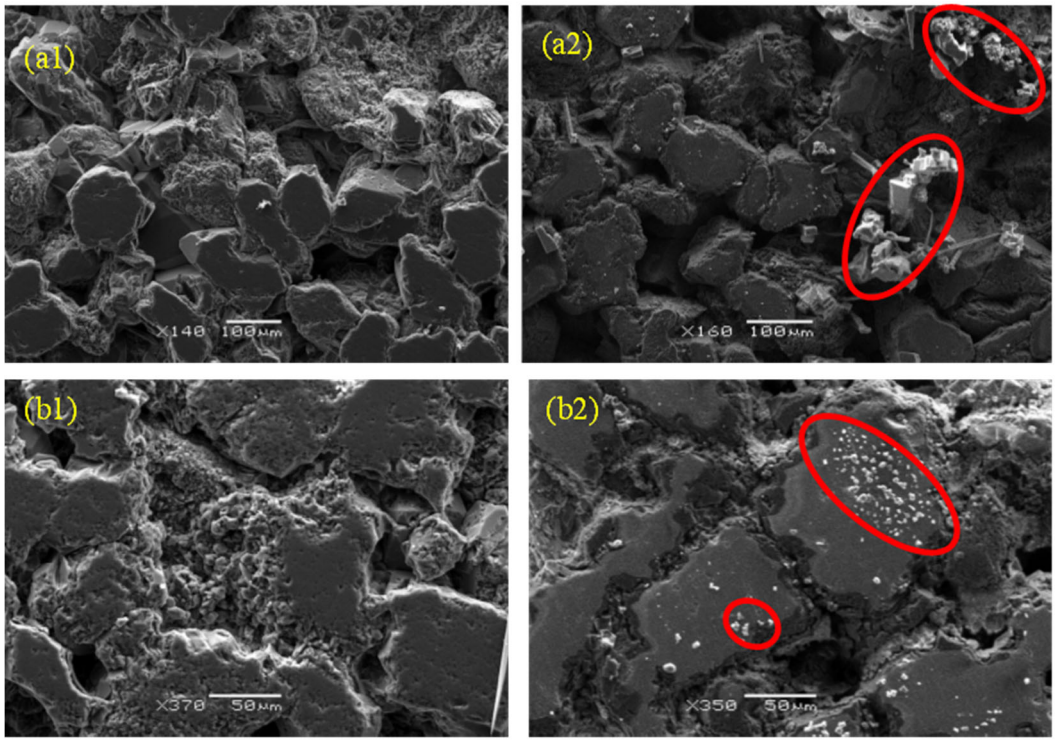

Figure 22. SEM images obtained before (**a1**,**b1**) and after aging in Hydrogen in an autoclave (**a2**,**b2**), showing the precipitation of halite minerals (red circle). Here, (**a1**,**a2**) are images of the BB sample and (**b1**,**b2**) are images of the BS sample.

The XRD measurements are also performed and compared with the pre-experiment mineralogical distribution. The changes in the mineralogy are shown in Table 6. Variations in mineral composition can be attributed to the heterogeneity of the rock samples.

Table 6. Comparison of the quantitative analyses of mineral composition obtained using the XRD method for the BB and BS samples, before and after the Hydrogen saturation experiment.

Sample	Before Experiment	After Experiment
BB	Quartz 80.1% Plagioclase 3.3% Potassium Feldspar 9.3% Kaolinite 7.3%	Quartz 81.7% Plagioclase 2.5% Potassium Feldspar 8.1% Kaolinite 4.1% Halite 0.8% Mica + Illite 2.8%
BS	Quartz 76% Plagioclase 4.3% Potassium Feldspar 7.6% Mica + Illite 12.1%	Quartz 73.8% Plagioclase 4.4% Potassium Feldspar 8.1% Mica + Illite 9.7% Kaolinite 2.8% Halite 1.2%

The experimental results show that the injection of CO_2 and Hydrogen both cause precipitation of halite minerals and dissolution and precipitation of other minerals, depending on the formation's mineralogy. These mineralogical changes can impact the injectivity of fluids (CO_2 and Hydrogen) in a reservoir, thereby affecting its storage capacity.

When compared with the simulation results, the experimental observations show that the pH drop during CO_2 injection predicted in the model corresponds well with the experimentally observed dissolution of feldspars and kaolinite and the precipitation of halite, mica, and illite. Although the simulations showed minimal pH changes with Hydrogen injection, the experiments reveal that Hydrogen can still induce minor mineralogical alterations over the long term.

5. Discussion

The mechanistic modeling approach reveals distinct gas-specific dynamics under identical reservoir conditions. Hydrogen exhibits faster buoyant migration and higher-pressure buildup (256 bars peak vs. 203 bars peak for CO_2 at 5000 Sm^3/day and 329 bars peak vs. 274 bars for CO_2 at 11,000 Sm^3/day), due to its lower density and viscosity than CO_2, and negligible solubility in brine, forming a thin gas cap with minimal residual trapping. In contrast, CO_2 shows broader lateral spreading, density-driven convective mixing (i.e., formation of pH fingers from denser, acidic brine), and solubility trapping that mitigates overpressure development.

Geomechanically, both gases increase total vertical stress via poroelastic effects, primarily driven by pore-pressure increases. For CO_2, vertical stress increases to 286 bars at 5000 Sm^3/day and 423 bars at 11,000 Sm^3/day injection rate, while for Hydrogen it reaches 380 bars at 5000 Sm^3/day and 450 bars at 11,000 Sm^3/day injection rate. However, CO_2 dissolution reduces the response because of its lower solubility in brine than hydrogen. Pressures remain below the BHP limit for CO_2 in both normal flow and coupled geomechanical cases at both injection rates, and for Hydrogen under normal flow at both rates. The exception occurs for Hydrogen in the coupled geomechanical case at the higher injection rate, where the well shuts in after ~4 years due to reaching the BHP limit.

The experimental results complement the simulation predictions. CO_2-induced pH drop (to 4.4 from equilibrium CO_2-brine reactions) aligns with observed pH decrease during the coreflooding experiment and dissolution and precipitation of minerals. In contrast, Hydrogen's exposure results in a negligible pH change, matching the minor geochemical alterations. Halite precipitation due to evaporation and brine supersaturation is observed for both gases. This integrated approach—where simulations capture reservoir-scale dy-

namics and experiments confirm geochemical alterations—improves the understanding of the formation behavior under gas injection.

The present study has several limitations, including the use of closed, rigid boundary conditions (leading to conservative overpressure estimates), equilibrium pH assumptions without full reactive transport (underestimating kinetic effects), and averaging of properties. Experimentally, the difference between the dynamic and static setups introduces bias, emphasizing qualitative identification over quantitative matching.

Future work could incorporate analyses of rock failure/caprock stability (e.g., Mohr–Coulomb criteria) to support a comprehensive leakage risk assessment. Additional extensions may include the pseudo-connections [35] for complex well configurations and reservoir heterogeneity, reactive transport modeling for long-term mineralization, and open-boundary analyses to refine pressure predictions.

6. Conclusions

This study represents an integrated simulation–experimental analysis of CO_2 and Hydrogen flow behavior, geomechanical response, and geochemical impacts in the Syderiai saline aquifer, addressing key gaps in Lithuanian reservoir assessments for CCUS and UHS.

The plume migration behavior is observed over 5 years of injection, with a 5-year monitoring period, and its impact on pH, pressure evolution, and gas saturation is documented. It is observed that the CO_2 and Hydrogen exhibit different behaviors in fluid migration and geochemical studies. The pH variation is more prominent during CO_2 injection, with a strong low-pH zone forming around the injection well. In contrast, Hydrogen shows negligible pH change even after 5 years of injection, confirming that it is a nonreactive, weakly soluble gas under reservoir conditions. The gas saturation variation shows a rapid rise and extensive spread of Hydrogen at the caprock-formation interface due to its lower density and viscosity than CO_2. Additionally, both gases showed pressure buildup due to injection into the reservoir, but they differ in their impact on the reservoir. CO_2 showed a moderate increase in pressure and a gradual increase in vertical stress, whereas Hydrogen showed a sharper rise in pressure and a rapid increase in vertical stress due to its low solubility and high mobility.

The mineralogical changes are observed through SEM image analyses and XRD measurements performed after the CO_2 coreflooding experiment and the saturation of Hydrogen in an autoclave. The halite precipitation is observed for both CO_2 and Hydrogen. In addition, precipitation and dissolution of other minerals are observed, including the dissolution and recrystallization of quartz, precipitation of clay minerals, and dissolution of feldspar.

Overall, the study provides an understanding of the flow patterns, dissolution behavior, geomechanical response, and geochemical impacts of both CO_2 and Hydrogen, which are important for CCS and UHS techniques that are key to the energy transition. Although the two gases differ significantly in their physical and chemical properties, the results indicate that deep saline aquifers can be considered viable storage options for both, subject to further investigation to address the identified limitations. This helps in designing safe injection strategies, assessing associated storage risks, and evaluating the suitability of reservoirs for long-term storage of the gases, thereby contributing to global energy security goals.

Author Contributions: Conceptualization, M.P.; methodology, S.M., P.A. and M.P.; software, P.A. and S.M.; validation, S.M., P.A. and M.P.; investigation, M.P.; resources, M.P.; data curation, S.M. and P.A.; writing—original draft preparation, S.M., P.A. and M.P.; writing—review and editing, S.M., P.A. and M.P.; visualization, S.M., P.A. and M.P.; supervision, M.P.; project administration, M.P.;

funding acquisition, S.M. and M.P. All authors have read and agreed to the published version of the manuscript.

Funding: This research was funded by the Lithuanian Research Council for postdoctoral research, proposal registration no. P-PD-22-022.

Data Availability Statement: The data presented in this study are available on request from the corresponding author.

Acknowledgments: The authors would like to acknowledge the Rock and Fluid Multiphysics Laboratory at the Department of Earth Sciences, IIT Roorkee, India, and the Polish Oil and Gas Institute for performing XRD and SEM measurements, and the Geo-energy lab at Kaunas University of Technology for providing computational resources.

Conflicts of Interest: The authors declare no conflicts of interest.

Abbreviations

The following abbreviations are used in this manuscript:

BSR	Baltic Sea Region
CCS	Carbon Capture and Storage
CCUS	Carbon Capture, Utilization, and Storage
EDS	Energy Dispersive X-ray Spectroscopy
FVM	Finite Volume Method
MRST	MATLAB Reservoir Simulation Toolbox
NMR	Nuclear Magnetic Resonance
SEM	Scanning Electron Microscopy
UHS	Underground Hydrogen Storage
XRD	X-ray Diffraction

References

1. *Sustainable Development Goals (SDG) Report; Progress Towards the Sustainable Development Goals*; General Assembly Economic and Social Council: New York, NY, USA, 2024; p. 12.
2. Shogenova, A.; Sliaupa, S.; Shogenov, K.; Vaher, R.; Sliaupiene, R. Geological Storage of CO_2—Prospects in the Baltic States. In Proceedings of the 69th EAGE Conference and Exhibition, London, UK, 11–14 June 2007.
3. Anthonsen, K.; Christensen, N. EU Geological CO_2 Storage Summary. In *Geological Survey of Denmark and Greenland for Clean Air Task Force*; Tech. Rep.; Geological Survey of Denmark and Greenland; Danish Ministry of Climate Energy and Utilities: Copenhagen, Denmark, 2021.
4. Shogenova, A.; Šliaupa, S.; Shogenov, K.; Šliaupiene, R.; Pomeranceva, R.; Vaher, R.; Uibu, M.; Kuusik, R. Possibilities for geological storage and mineral trapping of industrial CO_2 emissions in the Baltic region. *Energy Procedia* **2009**, *1*, 2753–2760. [CrossRef]
5. Šliaupienė, R.; Šliaupa, S. Prospects for CO_2 geological storage in deep saline aquifers of Lithuania and adjacent territories. *Geologija* **2011**, *53*, 121–133. [CrossRef]
6. Pal, M.; Malik, S.; Karaliūtė, V.; Makauskas, P.; Sharma, R. Assessing the Feasibility of Carbon Capture and Storage Potential in Lithuanian Geological Formations: A Simulation-based Assessment. In Proceedings of the 84th European Association of Geoscientists and Engineers (EAGE) Annual Conference & Exhibition, Vienna, Austria, 5–8 June 2023. [CrossRef]
7. Malik, S.; Makauskas, P.; Karaliūtė, V.; Pal, M.; Sharma, R. Assessing the Geological Storage Potential of CO_2 in Baltic Basin: A Case Study of Lithuanian Hydrocarbon and Deep Saline Reservoirs. *Int. J. Greenh. Gas Control.* **2024**, *133*, 104097. [CrossRef]
8. Malik, S.; Makauskas, P.; Sharma, R.; Pal, M. Evaluating Petrophysical Properties Using Digital Rock Physics Analysis: A CO_2 Storage Feasibility Study of Lithuanian Reservoirs. *Appl. Sci.* **2024**, *14*, 10826. [CrossRef]
9. Wu, J.; Ansari, U. From CO_2 sequestration to Hydrogen storage: Further utilization of depleted gas reservoirs. *Reserv. Sci.* **2025**, *1*, 19–35. [CrossRef]
10. Verma, A.; Malik, S.; Pal, M. Evaluating the potential for underground Hydrogen storage (UHS) in Lithuania: A review of geological viability and storage integrity. *Appl. Sci.* **2025**, *15*, 1614. [CrossRef]
11. Raad, S.M.J.; Leonenko, Y.; Hassanzadeh, H. Hydrogen storage in saline aquifers: Opportunities and challenges. *Renew. Sustain. Energy Rev.* **2022**, *168*, 112846. [CrossRef]

12. Katz, B.J. An overview of hydrogen in the subsurface. *Unconv. Resour.* **2025**, *8*, 100245. [CrossRef]
13. Ali, M.; Isah, A.; Yekeen, N.; Hassanpouryouzband, A.; Sarmadivaleh, M.; Okoroafor, E.R.; Kobaisi, M.A.; Mahmoud, M.; Vahrenkamp, V.; Hoteit, H. Recent progress in underground hydrogen storage. *Energy Environ. Sci.* **2025**, *18*, 5740–5810. [CrossRef]
14. Wen, G.; Benson, S.M. CO_2 plume migration and dissolution in layered reservoirs. *Int. J. Greenh. Gas Control* **2019**, *87*, 66–79. [CrossRef]
15. Wang, Q.; Zhang, D.; Li, Y.; Li, C.; Tang, H. Numerical simulation study of CO_2 storage capacity in deep saline aquifers. *Sci. Technol. Energy Transit.* **2024**, *79*, 12. [CrossRef]
16. Wang, C.; Wang, Z.; Li, H. Numerical modelling of CO_2 injection and storage in low porosity and low permeability saline aquifers: A design for the Permian Shiqianfeng formation in the Yulin area, Ordos Basin. *Sustainability* **2024**, *16*, 10593. [CrossRef]
17. Wang, G.; Pickup, G.; Sorbie, K.; Mackay, E. Numerical modelling of H_2 storage with cushion gas of CO_2 in subsurface porous media: Filter effects of CO_2 solubility. *Int. J. Hydrogen Energy* **2022**, *47*, 28956–28968. [CrossRef]
18. Ren, B.; Jensen, J.; Duncan, I.; Lake, L. Buoyant flow of H_2 vs. CO_2 in storage aquifers: Implications to geological screening. *SPE Reserv. Eval. Eng.* **2023**, *26*, 1048–1058. [CrossRef]
19. Wang, S.; Pan, S.; Tang, Y.; Gao, Y.; Wang, K. Experimental study of hydrogen flow behavior in sandstone at the core scale during cyclic hydrogen and water injections. *J. Energy Storage* **2025**, *123*, 116810. [CrossRef]
20. Bacci, G.; Korre, A.; Durucan, S. An experimental and numerical investigation into the impact of dissolutions/precipitation mechanisms on CO_2 injectivity in the wellbore and far field regions. *Int. J. Greenh. Gas Control.* **2011**, *5*, 579–588. [CrossRef]
21. Bacci, G.; Korre, A.; Durucan, S. Experimental investigation into salt precipitation during CO_2 injection in saline aquifers. *Energy Procedia* **2011**, *4*, 4450–4456. [CrossRef]
22. Jeddizahed, J.; Rostami, B. Experimental investigation of injectivity alteration due to salt precipitation during CO_2 sequestration in saline aquifers. *Adv. Water Resour.* **2016**, *96*, 23–33. [CrossRef]
23. Akindipe, D.; Saraji, S.; Piri, M. Salt precipitation during geological sequestration of supercritical CO_2 in saline aquifers: A pore-scale experimental investigation. *Adv. Water Resour.* **2021**, *155*, 104011. [CrossRef]
24. Malik, S.; Khan, M.S.; Pal, M.; Gomari, S.R.; Rahman, M.A.; Emad, W.A.S. Experimental Analysis of Geochemical Changes Caused by CO_2 Injection: A Study of Lithuanian Saline Aquifers. In Proceedings of the ADIPEC, Abu Dhabi, United Arab Emirates, 4–7 November 2024. [CrossRef]
25. Malik, S.; Khan, M.S.; Pal, M.; Gomari, S.R.; Rahman, M.A.; Sharma, R. Geochemical transformations induced by CO_2 injection in Lithuanian saline aquifers: Implications for carbon sequestration. 2025, *manuscript in preparation*.
26. Dabbaghi, E.; Ng, K.; Brown, T.C.; Yu, Y. Experimental study on the effect of hydrogen on the mechanical properties of hulett sandstone. *Int. J. Hydrogen Energy* **2024**, *60*, 468–478. [CrossRef]
27. Hassanpouryouzband, A.; Adie, K.; Cowen, T.; Thaysen, E.M.; Heinemann, N.; Butler, I.B.; Wilkinson, M.; Edlmann, K. Geological Hydrogen storage: Geochemical reactivity of Hydrogen with sandstone reservoirs. *ACS Energy Lett.* **2022**, *7*, 2203–2210. [CrossRef]
28. Vytyaz, O.; Chernova, O.; Stavychnyi, Y.; Martyniuk, R.; Ziaja, J. Increasing the reliability of oil and gas well fastening with polycomponent plugging systems. *Min. Miner. Depos.* **2024**, *18*, 82–93. [CrossRef]
29. Moore, D.M.; Reynolds, R.C., Jr. *X-Ray Diffraction and the Identification and Analysis of Clay Minerals*; Oxford University Press: Oxford, UK, 1989; pp. 179–201.
30. Srodon, J. X-Ray Powder Diffraction Identification of Illitic Minerals. *Clays Clay Miner.* **1984**, *32*, 337–349. [CrossRef]
31. Reynolds, R., Jr. *NEWMOD: A Computer Program for the Calculation of One-Dimensional Diffraction Patterns of Mixed-Layered Clays*; 8 Brook Rd.: Hanover, Germany, 1985.
32. Haselton, T.M. Minijos Nafta Clean Energy Project. In Proceedings of the Baltic Carbon Forum, Tallinn, Estonia, 22–23 October 2019.
33. T-Navigator. Academic License Provided by Rock Flow Dynamics, Inc., Version 25.2. Available online: https://rfdyn.com/tnavigator-25-2-key-updates-now-available/ (accessed on 2 November 2025).
34. Molina, O.; Vilarrasa, V.; Zeidouni, M. Geologic carbon storage for shale gas recovery. *Energy Procedia* **2017**, *114*, 5748–5760. [CrossRef]
35. Lukin, O.; Kondrat, O. Utilizing well-reservoir pseudo-connections for hydraulic fracturing modeling in tight gas saturated formations. *Min. Miner. Depos.* **2024**, *18*, 113–121. [CrossRef]